Effect of surrounding tissue on propagation of axisymmetric waves in arteries

K. Jagielska,[1,*] D. Trzupek,[1,2] M. Lepers,[1,3] A. Pelc,[4,†] and P. Zieliński[1,5]
[1]*The H. Niewodniczański Institute of Nuclear Physics PAN, ulica Radzikowskiego 152, 31-342 Kraków, Poland*
[2]*Institute of Physics, Jagiellonian University, ulica Reymonta 4, 30-059 Kraków, Poland*
[3]*UFR de Physique, Université de Lille 1, 59655 Villeneuve d'Ascq Cédex, France*
[4]*Collegium Medicum Jagiellonian University, ulica Św. Anny 12, 31-008 Kraków*
[5]*Institute of Physics, Cracow University of Technology, ulica Podchorążych 1, 30-084 Kraków, Poland*
(Received 27 July 2007; revised manuscript received 15 October 2007; published 7 December 2007)

A model of an artery consisting of a thin-walled flexible tube filled with a Newtonian incompressible liquid and surrounded by an external viscoelastic tissue is studied. The dispersion relations and attenuation lengths are determined for the lowest axially symmetric propagation modes: the Young, Lamb, and torsional modes. The numerical calculations confirm a low attenuation of the Young mode and a relatively weak dependence of its phase velocity on the elastic parameters of the surrounding medium. The Lamb and torsional modes show a nonzero frequency (a gap) at zero wave vector except for the limiting case of the absence of surroundings. The attenuation of the Lamb mode at zero frequency and the gap frequency turns out to be particularly sensitive to the elastic parameters of the surroundings. However, the spatial attenuation of the Lamb mode extends over a length of the order of 10 cm at the viscoelastic parameters corresponding to human tissues. Such lengths are comparable to the size of human organs. Three kinds of local axially symmetric perturbations have been studied, and the corresponding amplitude ratios of the Lamb to the Young mode calculated. The amplitude of the Lamb mode turns out to exceed that of the Young mode by a factor of ten at some frequencies with perturbations involving axial motions. Physiological consequences of this effect are discussed.

DOI: 10.1103/PhysRevE.76.066304 PACS number(s): 47.63.−b, 68.08.−p, 46.40.−f

I. INTRODUCTION

The blood flow in arteries consists of two components, steady and pulsatile [1–3]. The pulsatile flow predominates in the aorta and in larger arteries, whereas flow becomes practically continuous in the capillaries [4]. The larger arteries can thus be treated as waveguides conducting the initial forward waves and the backward waves reflected at bifurcations. Most existing work treats the waveguides as monomode. The only mode under consideration, called the Young mode, shows a linear dispersion relation with a relatively weak damping. The phase speed of this mode ranges from 5 to 15 m/s [1,2,5], whereas the heart beat frequency is somewhat higher than 1 Hz. This means that the wavelength of the fundamental harmonic (first harmonic) wave is about 5–15 m. The real pulse waves then are wave packets containing very many harmonics of the fundamental wave. Although the spatial extent of the entire wave of the Young mode packet is of the order of magnitude of meters, the phenomena of propagation and reflection of waves are of vital importance in the diagnostics of cardiovascular diseases [4,6]. In the present work, we use linearized Navier-Stokes equations valid in the long-wavelength limit [7].

The main issue of this work concerns the excitation of different harmonic waves (modes) by simple motions of the surrounding tissues. The main unexpected result is that a mode known as the Lamb mode, neglected in many existing analyses, becomes excited with rather high amplitude by quite simple and physiologically conceivable motions. The details of the model are described in Sec. II. Section III presents the derivation of the equations giving the dispersion relations of the axisymmetric modes supported by the model. The quantities characteristic of the modes and of their dispersion relations are presented in Sec. IV, and the method of obtaining the amplitudes of the modes generated by three kinds of local periodic perturbation is discussed in Sec. V. Section VI contains numerical results for the velocity profiles, dispersion relations, attenuation lengths, and excited amplitudes obtained with the model parameters corresponding to human arteries in various surrounding tissues. Section VII summarizes the results obtained, their physiological significance, and prospects for further studies.

II. THE MODEL

An artery is modeled here by an elastic thin-walled tube of inner radius a, thickness h, $h/a \ll 1$, and density ρ_w. Its Young modulus is E and Poisson ratio σ. The tube is filled with a Newtonian incompressible liquid of mass density ρ and dynamic viscosity μ. The outer medium, being a model of the tissue surrounding the vessel, is bounded by an external infinitely rigid and heavy tube coaxial with the artery, so its thickness is d. The geometry of the model is schematized in Fig. 1. The restoring forces and internal friction of the outer medium are described by three complex elastic parameters K_z, K_r, and K_θ and discussed in more detail in Sec. III. The axial motions of the surrounding medium are decoupled here from the radial motions at any wavelength, in contrast with an analogous thick-walled vessel model where they are decoupled at $k=0$ only. Despite this simplification, the model may reflect the real physiological situation of the outer medium, e.g., sliding on another layer of muscles or bones.

*Corresponding author. Katarzyna.Jagielska@ifj.edu.pl
†Deceased.

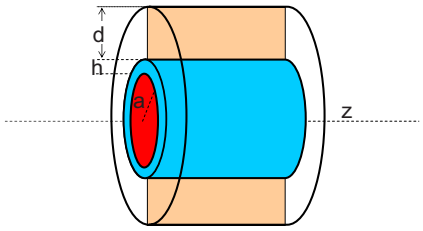

FIG. 1. (Color online) Geometry of model.

The model shows a symmetry of the point group $D_{\infty h}$ (∞/mmm) and, in addition, is invariant by any translation along the vessel axis. All the normal modes are classified by the irreducible representations of this group. Consequently, the z and θ dependence of every mode is given by a phase factor $\exp(ikz+in_\theta\theta)$, where the wave vectors $k>0$ characterize the modes propagating in the positive direction and $k<0$ the backward modes, while the azimuthal wave number n_θ is a discrete variable, $n_\theta=0,1,\ldots,\infty$.

III. GOVERNING EQUATIONS AND BOUNDARY CONDITIONS

A. Equations of motion of the fluid and general form of the velocity field

A Newtonian liquid obeys the momentum equation (Navier-Stokes equation)

$$\frac{\partial\vec{v}}{\partial t}+\vec{v}\cdot\vec{\nabla}\vec{v}=-\frac{1}{\rho}\vec{\nabla}p+\frac{\mu}{\rho}\Delta\vec{v} \tag{1}$$

and the continuity equation of an incompressible liquid

$$\vec{\nabla}\cdot\vec{v}=0. \tag{2}$$

The quantity p is the excess pressure of the liquid over a constant equilibrium value. The nonlinear term $\vec{v}\cdot\vec{\nabla}\vec{v}$ is neglected in the approximation of small vibrations and long wavelengths. When applied to Eq. (1) so linearized, the divergence operator produces the pressure as a harmonic function [8], i.e.,

$$\Delta p=0. \tag{3}$$

In cylindrical coordinates and with $n_\theta=0$, the linearized Navier-Stokes equation (1) reads

$$\frac{\partial v_z}{\partial t}=-\frac{1}{\rho}\frac{\partial p}{\partial z}+\frac{\mu}{\rho}\left(\frac{\partial^2 v_z}{\partial z^2}+\frac{\partial^2 v_z}{\partial r^2}+\frac{1}{r}\frac{\partial v_z}{\partial r}\right), \tag{4}$$

$$\frac{\partial v_r}{\partial t}=-\frac{1}{\rho}\frac{\partial p}{\partial r}+\frac{\mu}{\rho}\left(\frac{\partial^2 v_r}{\partial z^2}+\frac{\partial^2 v_r}{\partial r^2}+\frac{1}{r}\frac{\partial v_r}{\partial r}-\frac{v_r}{r^2}\right), \tag{5}$$

$$\frac{\partial v_\theta}{\partial t}=\frac{\mu}{\rho}\left(\frac{\partial^2 v_\theta}{\partial z^2}+\frac{\partial^2 v_\theta}{\partial r^2}+\frac{1}{r}\frac{\partial v_\theta}{\partial r}-\frac{v_\theta}{r^2}\right). \tag{6}$$

The continuity equation [Eq. (2)] is then

$$\frac{\partial v_z}{\partial z}+\frac{\partial v_r}{\partial r}+\frac{v_r}{r}=0. \tag{7}$$

The component v_θ is entirely decoupled from the remaining components of the liquid velocity as a result of the symmetry of the system.

With the wave ansatz $p(z,r,t)=P(r)\exp(-i\omega t+ikz)$ and $v_q(z,r,t)=V_q(r)\exp(-i\omega t+ikz)$, $q=z,r,\theta$, Eq. (3) reduces to the Bessel equation having as a solution finite at $r=0$

$$P(r)=BJ_0(ikr), \tag{8}$$

where $J_0(ikr)$ is the Bessel function of the first kind, and Eqs. (4)–(6) give

$$V_z(r)=\frac{Bk}{\rho\omega}J_0(ikr)+CJ_0(\alpha_k r), \tag{9}$$

$$V_r(r)=-\frac{Bk}{\rho\omega}J_1(ikr)+\frac{ikC}{\alpha_k}J_1(\alpha_k r), \tag{10}$$

$$V_\theta(r)=DJ_1(a_k r), \tag{11}$$

where

$$\alpha^2=\frac{i\omega\rho}{\mu}-k^2. \tag{12}$$

The coefficients B, C, and D are to be determined by boundary conditions. The torsional motion is decoupled from V_z and V_r by symmetry.

B. Motion of the vessel wall and boundary conditions

The cylindrical components of the displacement vector $u_z(z,r=a,t)$, $u_r(z,r=a,t)$, and $u_\theta(z,r=a,t)$ of the vessel wall obey the following system of equations:

$$h\rho_w\frac{\partial^2 u_z}{\partial t^2}=hE_\sigma\left(\frac{\partial^2 u_z}{\partial z^2}+\frac{\sigma}{a}\frac{\partial u_r}{\partial z}\right)-\mu\left(\frac{\partial v_z}{\partial r}+\frac{\partial v_r}{\partial z}\right)-\frac{K_z'}{d}u_z-\frac{K_z''}{d}\frac{\partial u_z}{\partial t}, \tag{13}$$

$$h\rho_w\frac{\partial^2 u_r}{\partial t^2}=p-2\mu\frac{\partial v_r}{\partial r}-\frac{hE_\sigma}{a}\left(\frac{u_r}{a}+\sigma\frac{\partial u_z}{\partial z}\right)-\frac{K_r'}{d}u_r-\frac{K_r''}{d}\frac{\partial u_r}{\partial t}, \tag{14}$$

$$h\rho_w\frac{\partial^2 u_\theta}{\partial t^2}=\frac{hE}{2(1+\sigma)}\frac{\partial^2 u_\theta}{\partial z^2}-\mu\left(\frac{\partial v_\theta}{\partial r}-\frac{v_\theta}{a}\right)-\frac{K_\theta'}{d}u_\theta-\frac{K_\theta''}{d}\frac{\partial u_\theta}{\partial t}, \tag{15}$$

where

$$E_\sigma=\frac{E}{1-\sigma^2}. \tag{16}$$

The stresses exerted by the flowing liquid on the inner surface of the vessel wall are proportional to the liquid velocity gradient field [9]. The explicit form of Eqs. (13)–(15) helps

to realize the properties of the outer medium in the present model. This is, namely, a kind of metamaterial, which consists of rods sticking inward from the outermost rigid tube (see Fig. 1) in the radial direction. The parameters K_r' and K_r'' are the restoring force constant (Young modulus) and the damping constant, respectively, which are related to the longitudinal elongation or compression of the rods. The rods are supposed to be attached to the outer rigid tube on a kind of elastic articulations so that there exist restoring forces proportional to the tilt angles. The forces may also be interpreted as the ones acting on the surroundings when it slides harmonically on still more outer tissue. The lack of elongation stiffness constants in the directions z and θ as well as of a mass density of the outer medium may be plausibly absorbed in the elastic properties and in the mass density of the vessel wall.

The nonslip boundary conditions between the liquid and the vessel wall are

$$\frac{\partial u_z}{\partial t} = v_z|_{r=a}, \tag{17}$$

$$\frac{\partial u_r}{\partial t} = v_r|_{r=a}, \tag{18}$$

$$\frac{\partial u_\theta}{\partial t} = v_\theta|_{r=a}. \tag{19}$$

As in the case of the liquid velocity, the vessel wall displacement has a wave form $u_z = Ze^{-i\omega t+ikz}$, $u_r = Re^{-i\omega t+ikz}$, and $u_\theta = Te^{-i\omega t+ikz}$.

IV. DISPERSION RELATIONS OF THE LOWEST MODES

With the wave ansatz adopted, the amplitudes B, C, D [Eqs. (8)–(11)] and Z, R, T have to satisfy a system of homogeneous linear equations which for symmetry reasons splits into two independent parts as written below in matrix form:

$$[M_1]\begin{bmatrix} Z \\ R \\ B \\ C \end{bmatrix} = 0, \tag{20}$$

with

$$M_1 = \begin{bmatrix} \rho_w\omega^2 - E_\sigma k^2 - \tilde{K}_z & \frac{ik\sigma E_\sigma}{a} & -\frac{k^3 a\mu}{\omega\rho h} & \left(1 - \frac{k^2a^2}{\Lambda^2}\right)J_1(\Lambda)\frac{\mu\Lambda}{ha} \\ \frac{-ik\sigma E_\sigma}{a} & \rho_w\omega^2 - \frac{E_\sigma}{a^2} - \tilde{K}_r & \frac{1}{h} + \frac{ik^2\mu}{h\omega\rho} & \frac{2ik\mu}{h}\left(J_0(\Lambda) - \frac{J_1(\Lambda)}{\Lambda}\right) \\ i\omega & 0 & \frac{k}{\omega\rho} & J_0(\Lambda) \\ 0 & i\omega & -\frac{iak^2}{2\omega\rho} & -\frac{ika}{\Lambda}J_1(\Lambda) \end{bmatrix} \tag{21}$$

and

$$[M_2]\begin{bmatrix} T \\ D \end{bmatrix} = 0, \tag{22}$$

with

$$M_2 = \begin{bmatrix} \rho_w\omega^2 - \frac{Ek^2}{2(1+\sigma)} - \tilde{K}_\theta\frac{\Lambda\mu}{ha}\left(\frac{2J_1(\Lambda)}{\Lambda} - J_0(\Lambda)\right) \\ i\omega \quad J_1(\Lambda) \end{bmatrix}, \tag{23}$$

where the following abbreviations have been adopted: $\Lambda = \alpha_k a$ and $\tilde{K}_q = (1/hd)(K_q' - i\omega K_q'')$, while $q = z, r, \theta$.

In the long-wavelength limit $ka \ll 1$, the Bessel functions are approximated by $J_0(ikr) \approx 1$ and $J_1(ikr) \approx ikr/2$, which produces a flat pressure profile $P(r) = B$ [see Eq. (8)] and $\alpha_k \approx \alpha = (i+1)\sqrt{\omega\rho/2\mu}$.

The condition $\det(M_1) = 0$ gives the dispersion relations for the modes involving axial and radial motions of the vessel wall, traditionally called Young ($i=1$) and Lamb ($i=2$) modes [10], whereas $\det(M_2) = 0$ defines the dispersion relation of the torsional mode.

To solve the system of equations (20) with the singular matrix M_1 [Eq. (21)], we express the amplitudes C_i, R_i, and Z_i ($i = 1, 2$) by the pressure amplitude B_i selected as independent (no summation implied):

$$C_i = W_{Ci}B_i, \tag{24}$$

$$Z_i = W_{Zi}B_i, \tag{25}$$

$$R_i = W_{Ri}B_i. \tag{26}$$

When inserted into Eqs. (9) and (10) the amplitudes resulting from Eqs. (24)–(26) determine the velocity profiles corresponding to each mode. They also determine the amplitudes

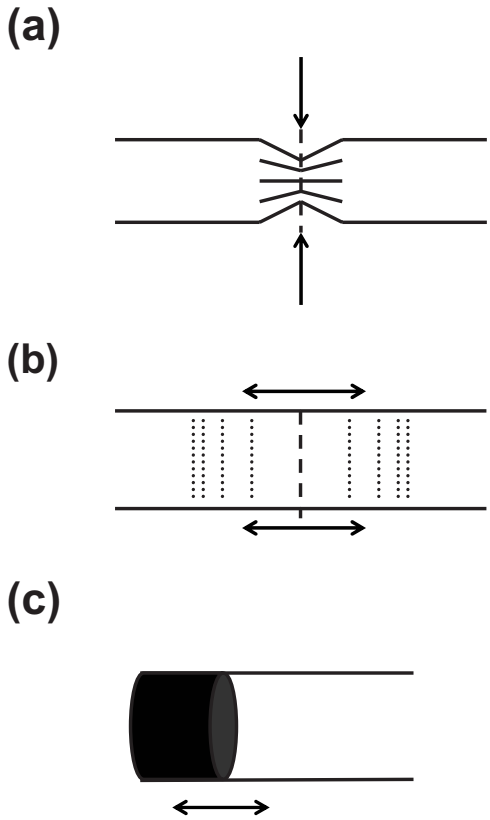

FIG. 2. Schemes of excitation of modes by circular contraction (a), by axial displacement (b), and by a pistonlike movement (c).

of the vessel wall motions. An analogous analysis of the system of equations (22) provides the profile of the azimuthal velocity given directly by Eq. (11).

V. EXCITATION OF MODES BY SIMPLE LOCAL PERTURBATIONS

We now wish to evaluate the amplitude ratios B_2/B_1 of the Lamb ($i=2$) and Young ($i=1$) modes excited in response to local axially symmetric perturbations corresponding to plausible physiological motions of the surrounding medium. Figure 2(a) represents an overall contraction-expansion motion at $z=0$ which affects only the radial component. Denoting by the subscript + the amplitudes of the modes propagating in the positive direction and by − the modes propagating in the negative direction, one finds $B_{1+}=B_{1-}$, $B_{2+}=B_{2-}$.

The continuity of the vessel wall in the radial direction requires that

$$R_{1+} + R_{2+} = R_{1-} + R_{2-} = R_0 = W_{R1}B_{1+} + W_{R2}B_{2+},$$

where R_0 is the amplitude of the local compression.

The continuity in the axial direction is expressed by $Z_{1+}+Z_{2+}=Z_{1-}+Z_{2-}=W_{Z1}B_{1+}+W_{Z2}B_{2+}=0$, which gives the desired ratio

$$B_{2+}/B_{1+} = -W_{Z1}/W_{Z2}. \tag{27}$$

The kind of excitation shown in Fig. 2(b) represents an axial vibration of amplitude Z_0, which is antisymmetric against reflection in the radial section, $Z_{1+}+Z_{2+}=-Z_{1-}-Z_{2-}=W_{Z1}B_{1+}+W_{Z2}B_{2+}=Z_0$.

We assume that the radius of the vessel does not change in this kind of perturbation, $R_{1+}+R_{2+}=R_{1-}+R_{2-}=W_{R1}B_{1+}+W_{R2}B_{2+}=0$, so that the amplitude ratio is

$$B_{2+}/B_{1+} = -W_{R1}/W_{R2}. \tag{28}$$

Another kind of mode excitation shown in Fig. 2(c) is also antisymmetric with respect to the radial section and is defined by the condition

$$C_{1+} + C_{2+} = C_{1-} + C_{2-} = W_{C1}B_{1+} + W_{C2}B_{2+} = 0.$$

This condition corresponds [see Eq. (9)] to an axial velocity constant in the whole cross section perpendicular to the axis [$J_0(ikr)\approx 1$ in the long-wavelength limit approximation]. Thus, this kind of motion resembles the action of a piston moving axially at the section $z=0$. Since the radial velocity then depends on the distance r from the axis the piston is perfectly slippery. The amplitude of this motion is given by $Z_{1+}+Z_{2+}=-Z_{1-}-Z_{2-}=W_{Z1}B_{1+}+W_{Z2}B_{2+}=Z_0$, and is accompanied by the appropriate variation of the vessel radius.

The interesting mode amplitude ratio now reads

$$B_{2+}/B_{1+} = -W_{C1}/W_{C2}. \tag{29}$$

As far as the torsional mode is concerned, there is only one type of symmetry-adapted excitation, i.e., a rotational one, and thus only this mode arises.

The most interesting is the kind of motion at the root of the aorta in the vicinity of the aortic valve. The most obvious component of this motion is the one resembling the action of a piston since an additional volume (stroke volume) is injected into the aorta. However, the profile of the axial velocity is surely not planar, so that the axial component involving independent displacement of the heart annulus is also excited. Less clear is a contraction-expansion annulus motion, which must also exist independently of the passive reaction to the radial blood velocity. A torsional motion, resembling the motion of a bullet in the rifled barrel of a gun, cannot be excluded either. In what follows all the kinds of motion are treated separately.

VI. NUMERICAL RESULTS

A. Motions involved in particular modes

We have solved the equations $\det(M_1)=0$ and $\det(M_2)=0$ [Eqs. (21) and (23)] using the parameters of the human ascending aorta [5] with the radius $a=0.0147$ m, wall thickness $h=0.001\,63$ m, and the Young modulus $E=0.4\times 10^6$ Pa. The vessel wall is close to being incompressible [1,10], i.e., $\sigma=0.5$. For the wall density we take the value $\rho_w=1055$ kg/m^3, but we have also studied the effect of its variation in a wide range from $\rho_w=940$ kg/m^3 (corresponding to the density of the adipose tissue) to $\rho_w=1975$ kg/m^3 (corresponding to the density of bones) [11,12]. This approach is all the more justified that the effective wall density accounts, to the extent implied by the adopted approximations, for the density of the tissue surrounding the vessel. The densities of various human tissues are presented in Table I

TABLE I. Densities of selected human tissues [10,11]

Material	Density (ρ_w) (kg m^{-3})
Bones	1975
Smooth muscle	1060
Brain	1030
Skin	1191
Tendons	1125
Adipose tissue	940
Mean value of density of human body	1055–1100

[10,11]. The parameters of the blood are the following: density $\rho=1055$ kg/m^3 and viscosity $\mu=0.0032$ Pa s [10,11]. The surrounding tissue is assumed to have a thickness d, which we take to be equal to the tube radius a, whereas the parameters K' correspond roughly to the Young moduli of human tissues and the damping parameters K'' are comparable with the blood viscosity. We have varied the parameters K' in a wide range from 5×10^3 Pa (Young modulus of adipose tissue) to 10^9 Pa (Young modulus of bones). The values of the parameters K' are collected in Table II [13,14].

The difference between the Young and Lamb modes is best visible when comparing their profiles of axial velocity. Whereas this velocity decreases almost (however, not exactly) to zero at the vessel wall in the case of the Young mode [Fig. 3(a)], it attains its maximum there in the Lamb mode [Fig. 3(b)]. Figures 3(a)–3(d) show the effect of the surrounding tissue on the velocity profiles of Young and Lamb modes. Generally, the axial velocity amplitude in the Young mode [Fig. 3(a)] decreases with increasing elastic modulus of the surrounding medium (at a given pressure amplitude B), whereas the velocity amplitude in the Lamb mode [Fig. 3(b)] increases and, moreover, in a more pronounced way. The profiles of the radial velocity are more complicated. They always start from zero at the axis [Figs. 3(c) and 3(d)]. The radial velocities in the Young mode at the vessel wall are generally much higher than in the Lamb mode. With increasing elastic modulus K' of the surroundings the radial velocity of the Young mode diminishes and

TABLE II. Young's modulus of selected human tissues [13,14]

Material	Young's modulus (E) (Pa)
Adipose tissue	5×10^3
Relaxed smooth muscle	6×10^3
Contracted smooth muscle	$(10-250)\times10^3$
Fibroglandular	5×10^4
Skin	5×10^5
Rubber	6.9×10^6
Fresh bone	20.685×10^6
Cartilage	24.13×10^6
Tendon	551.6×10^6
Bone	10^9

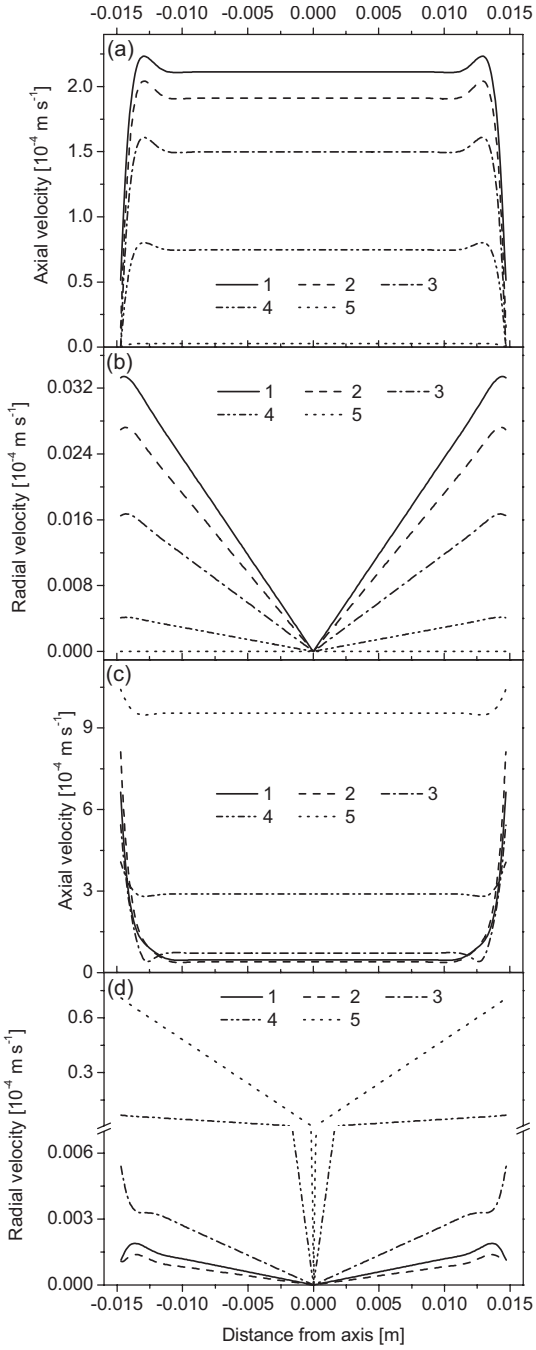

FIG. 3. Axial velocity profiles in Young mode (a) and in Lamb mode (c). Radial velocity profiles in Young mode (b) and Lamb mode (d) with various elastic parameters of surrounding medium. Particular curves correspond to the following values of parameter K'_z: $K'_z=$(1) 10^4, (2) 10^5, (3) 10^6, (4) 10^7, and (5) $K'_z=10^8$ Pa. Standard amplitude of pressure $B=1$ Pa. Parameters K'_r are $K'_r=3K'_z$; internal friction parameters are $K''_r=K''_z=0$.

that of the Lamb mode strongly grows [Figs. 3(c) and 3(d)], which means that the Lamb mode acquires a more and more radial character. The resulting enhanced bulging-shrinking motions of the vessel wall may result in an easer detectability of the Lamb mode by experiments and/or in its perceptibility by nervous receptors such as baroreceptors when the vessel is placed in elastic surroundings.

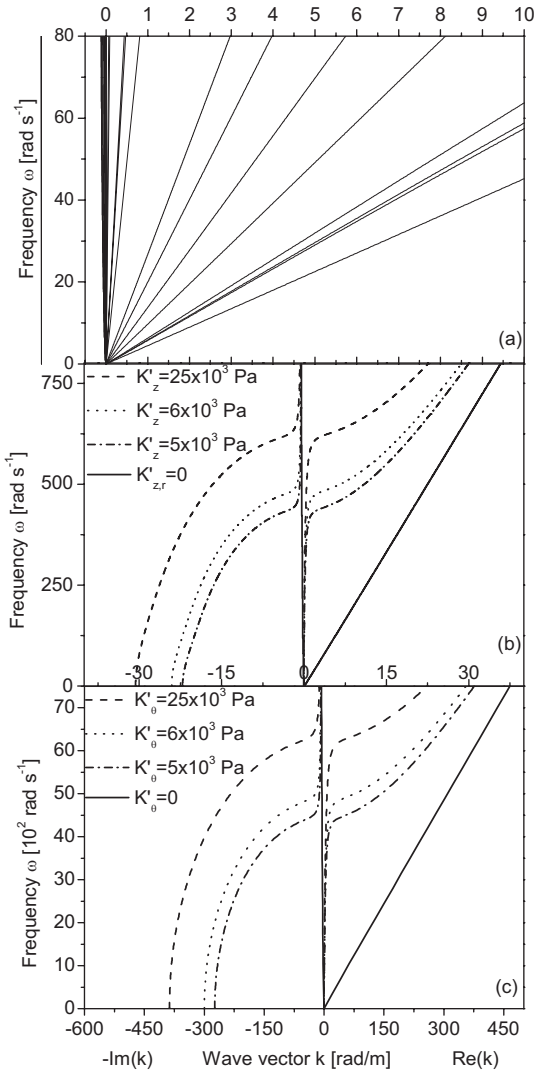

FIG. 4. Dispersion relations of Young mode (a), Lamb mode (b), and torsional mode (c) with various elastic parameters of surrounding medium, $K_r'=3K_z'$, $K_{z,r,\theta}''=0$, $\rho_w=1055$ kg/m^3. Positive part of abscissa corresponds to real part of wave vector, Re k, and negative part to attenuation coefficient Im k. (a) Lowest line corresponds to case without surrounding tissue and the subsequent lines correspond to the values of parameter $K_{z,\theta}$ 5×10^3, 6×10^3, 10×10^3, 5×10^4, 12×10^4, 25×10^4, 5×10^5, 69×10^5, 20.685×10^6, 24.13×10^6, 551.6×10^6, and 10^9 Pa.

B. Dispersion relations

Figures 4(a)–4(c) show the dispersion relations for the Young, Lamb, and torsional modes with various parameters of external tissues at vanishing internal friction $K_{z,r,\theta}=0$. The dispersion relations are presented here as the real frequencies ω dependent on the complex wave vector $k=\mathrm{Re}\,k+i\,\mathrm{Im}\,k$. The real part of the wave vector Re k is shown on the positive part of the abscissa, whereas the negative part of the abscissa represents the imaginary part Im k. The latter describes the spatial attenuation of the corresponding waves. In the case of the vessel without surroundings, we obtain the velocity of the Young mode 4.6 m/s, which agrees with that calculated from the Moens-Korteweg formula [5]. The

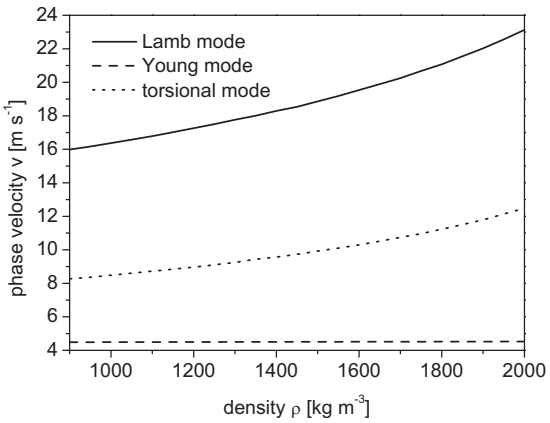

FIG. 5. Phase velocities of Young, Lamb, and torsional modes deduced from linear high-frequency parts of corresponding dispersion relation as functions of wall density ρ_w.

Young mode velocity increases with increasing rigidity of the surrounding tissue, and for the cases which correspond to the relaxed ($K_z'=6\times10^3$ Pa, $K_r'=3K_z'$) and contracted [$K_z'=(10-250)\times10^3$ Pa, $K_r'=3K_z'$] muscles, we obtain the wave velocity 6 m/s and from 6.4 to 10 m/s, respectively. The Lamb mode is more sensitive to the elastic properties of the surrounding tissue.

A qualitative difference of the Lamb mode as compared with the Young one is that the introduction of the surrounding tissue produces a gap on the axis of the imaginary part of the wave vector, i.e., the Lamb mode becomes highly damped, starting from the lowest frequencies. With increasing frequency the damping decreases, and starting from a quasithreshold value of frequency, about 400 rad/s for adipose tissue, 600 rad/s for contracted muscle, and 2×10^5 rad/s for bone tissue, the damping becomes weak so that the corresponding wave propagates for longer distances. This is a trace of an optical rather than acoustic character of the Lamb mode in terms of acoustic vs optical phonons in condensed matter. In fact, when traced as a function of the real wave vector, the real part of the frequency of the Lamb mode tends to a nonzero value at $k\to0$. An analogous behavior is seen in the case of the torsional mode, with, however, a stronger damping and, consequently, larger gap.

Introduction of internal friction parameters of the surroundings, $K_{z,r,\theta}''$, generally suppresses the gap on the imaginary part of the wave vector for all the modes. Variation of the wave speed then is relatively weak (not presented in figures here).

Figure 5 shows the propagation speeds of the three modes as functions of the wall density ρ_w. This dependence turns out to be fairly weak in the physiologically relevant range of this parameter.

The spatial extent of a damped mode is described by the inverse of the imaginary part of its wave vector. This quantity, called here the attenuation length (comparable to the transmission of Ref. [15]), is depicted in Figs. 6(a)–6(c) for the Young, Lamb, and torsional modes. This length exceeds by at least a factor of 5 the size of a human in the frequency range 0–100 rad/s in the case of the Young mode. Thus, this mode is practically undamped in the physiological range of

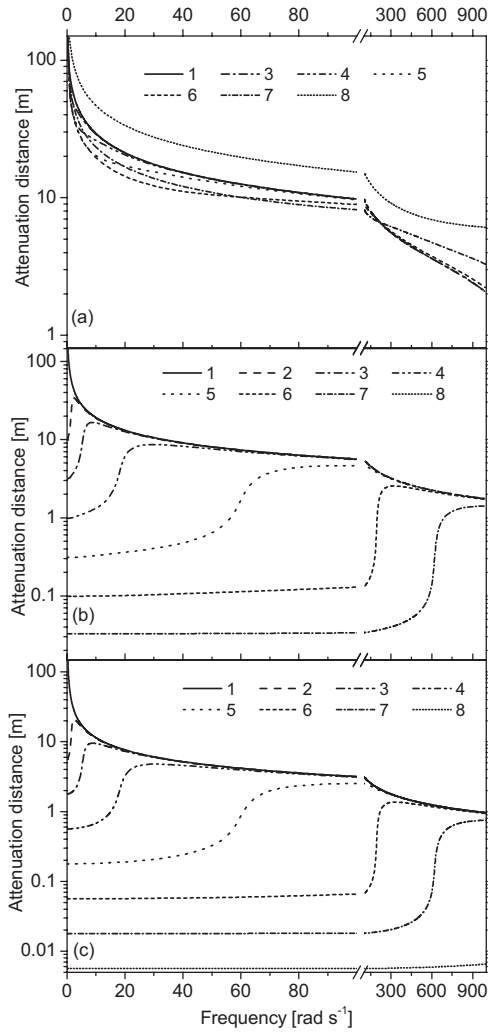

FIG. 6. Attenuation length $1/\mathrm{Im}\,k$ in Young mode (a), Lamb mode (b), and torsional mode (c) as function of frequency with selected surrounding parameters $K_z'=K_\theta'$, $K_r'=3K_z'$, $K_{z,r,\theta}''=0$, $\rho_w=1055\ \mathrm{kg/m^3}$. Particular curves correspond to the following values of parameter K_z': $K_z'=$(1) 0, (2) 0.1, (3) 1, (4) $K_z'=10$, (5) 10^2, (6) 10^3, (7) 10^4, and (8) 10^5.

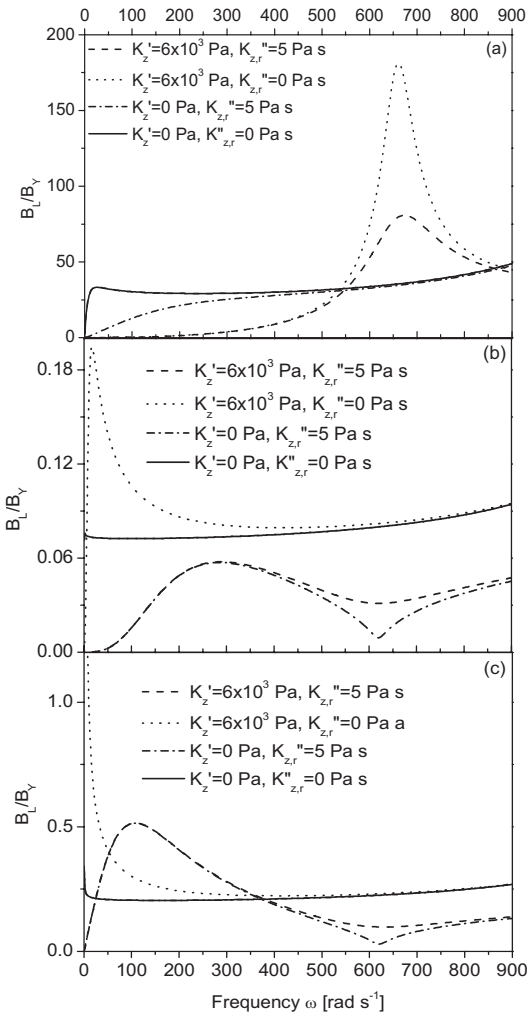

FIG. 7. Pressure amplitude ratio B_L/B_Y of Lamb to Young modes as function of frequency for modes generated by axial displacement (a), circular radial contraction (b), and pistonlike movement (c). Other parameters: $\rho_w=1055\ \mathrm{kg/m^3}$, $K_r'=3K_z'$.

frequencies. The spatial damping of the Lamb and torsional modes strongly depends on the surrounding medium. It is noteworthy that the attenuation lengths of the Lamb and torsional modes decrease only by a factor of 2–3 in the range of frequencies from 0 to about 100 rad/s, i.e., about the tenth harmonic of the fundamental pulse wave. Increasing the elastic parameter K_z' results in a strong reduction of the attenuation length in a more and more extended range of frequency. Nevertheless, we see, e.g., that at the elastic parameters close to the adipose ($K_z'=5\times10^3$ Pa) or relaxed smooth muscles tissue ($K_z'=6\times10^3$ Pa), this distance is still as long as about 10 cm in the frequency range 0–100 rad/s. Such a distance cannot be neglected in the size scale of a human or of internal organs

C. Excitation of the Young and Lamb modes

The pressure amplitude ratios B_L/B_Y excited in the three ways described in Sec. V are depicted in Figs. 7(a)–7(c) for selected sets of parameters. The most spectacular effect of the presence of the Lamb mode is visible in the axial type of local excitation [Fig. 7(a)]. In the absence of external tissue, the amplitude of the Lamb mode exceeds that of the Young mode by a factor of 35–60 in the whole region studied except for the very low-frequency range ~12 rad/s. Addition of purely elastic surroundings results in a suppression of the Lamb mode at low frequencies but, in turn, produces a high resonance peak related to the shear stiffness parameter of the medium, K_z'. As expected, the maximum of this peak is sensitive to the parameter K_z', whereas (as we have checked) the effect of other parameters is practically negligible.

VII. DISCUSSION

The results of the previous section confirm that of the modes with $n_\theta=0$ the least attenuated one is the Young mode. Therefore, it is mainly this mode that is palpable at wrist or neck arteries. The phase velocity of the Young mode is mainly dependent on the stiffness parameters of the vessel

wall and of the surrounding medium, whereas the internal friction affects the properties of this mode in a way that does not seem to have physiological importance. The effect of the increase in the wave speed with the stiffness of the vessel wall is well known [4]. An analogous effect of the surroundings of the vessel, e.g., cerebrospinal fluid, muscles, bones, etc., seems to be worth deeper physiological studies.

The main common property of the Lamb and torsional modes is that they show a frequency gap at $k=0$ in analogy to optic modes in solids. However (which is not presented here), when traced as a function of the real wave vector, the frequency of the Lamb mode happens to lose its real part at a nonzero wave vector at high enough internal friction of the surrounding medium. Waves longer than the corresponding limiting wavelength decay exponentially without any oscillation. Generally, the Lamb and torsional modes propagate to longer distances above a quasithreshold frequency, roughly corresponding to the $k=0$ gap, which increases with increasing stiffness of the surrounding medium. We have shown that the attenuation length of the Lamb mode may be of order of tens of centimeters in the frequency range comprising the main harmonics forming the wave packets of the pulse waves. Thus, once excited, this mode has a non-negligible amplitude in a significant portion of the artery. We have also shown that among local perturbations the most efficient one in exciting the Lamb mode is an axial annular motion. There exists then a resonant frequency related to the shear stiffness parameter of the surrounding medium. The effect is worth studying in thick walled models [16,17]. The amplitude of the Lamb mode excited at this frequency is particularly high. The attenuation length at the resonant frequency is comparable with the size of organs in humans. The extra pressure then produced by the Lamb mode may be perceptible by baroreceptors placed in those regions. Therefore, the high amplitude found in this case may have some physiological significance. Local perturbations may result, e.g., from motion in exercise or in locomotion as well as from internal factors, such as wave reflection or movements of neighboring organs. It seems that the predicted high amplitude of the Lamb mode excited in such cases deserves thorough theoretical and experimental studies.

ACKNOWLEDGMENTS

This work was partially supported by the MANAR network financed by the Ministry MNi SzW (Poland). The contribution of the cooperation project of Polish Academy of Sciences (PAN) and Centre National de la Recherche Scientifique (CNRS), France (Cooperation Contract No. 19503) is acknowledged.

[1] W. Milnor, *Hemodynamics*, 2nd ed. (Williams & Wilkins, Baltimore, 1989).
[2] W. Nichols and M. O'Rourke, *McDonald's Blood Flow in Arteries*, 5th ed. (Hodder Arnold, London, 2005).
[3] M. Zamir, *The Physics of Pulsatile Flow* (AIP Press, Sringer, New York, 2000).
[4] M. F. O'Rourke, J. Biomech. **36**, 623 (2003).
[5] J. J. Wang and K. H. Parker, J. Biomech. **37**, 457 (2004).
[6] H. Demiray, Int. J. Non-Linear Mech. **41**, 258 (2006).
[7] S. C. Ling, N. B. Atabek, W. G. Letzing, and D. J. Patel, Circ. Res. **33**, 198 (1973).
[8] J. C. F. Chow and J. T. Apter, J. Acoust. Soc. Am. **2**, 437 (1968).
[9] L. D. Landau and E. Lifshitz, *Course of Theoretical Physics: Mechanics of Continuous Media* (Pergamon Press, Oxford, 1981).
[10] K.-J Li John, *Arterial System Dynamics* (Columbia University Press, New York, 1987).
[11] A. Nowicki, *Foundations of Doppler Ultrasonography* (PWN, Warsaw, 1995) (in polish).
[12] M. Jeżewski and J. Kalisz, *Tables of Physical Quanities* (PWN, Warsaw, 1957) (in polish).
[13] Alan C. Burton, *Physiology and Biophysics of the Circulation; An Introductory Text* (Year Book Medical Publishers, Chicago, 1965).
[14] Y. C. Fung, *Biomechanics: Mechanical Properties of Living Tissues* (Springer-Verlag, New York, 1993).
[15] R. H. Cox, Biophys. J. **8**, 691 (1968).
[16] U. Dinnar, TIT J. Life Sci. **5**, 49 (1975).
[17] S. Cirovic, C. Walsh, and W. D. Fraser, J. Fluids Struct. **16**, 1029 (2002).